Laser desorption VUV postionization MS imaging of a cocultured biofilm

Authors: Chhavi Bhardwaj, Jerry F. Moore, Yang Cui, Gerald L. Gasper, Hans C. Bernstein, Ross P. Carlson, &Luke Hanle

Bhardwaj C, Moore JF, Cui Y, Gasper GL, Bernstein HC, Carlson RP, Hanley L, "Laser desorption VUV postionization MS imaging of a cocultured biofilm," Analytical and Bioanalytical Chemistry. September 2013 405(22):6969-77

Laser desorption VUV postionization MS imaging of a cocultured biofilm

Chhavi Bhardwaj, Jerry F. Moore, Yang Cui, Gerald L. Gasper, Hans C. Bernstein, Ross P. Carlson, & Luke Hanley

Abstract

Laser desorption postionization mass spectrome-try (LDPI-MS) imaging is demonstrated with a 10.5 eV photon energy source for analysis and imaging of small endogenous molecules within intact biofilms. Biofilm con-sortia comprised of a synthetic Escherichia coli K12 cocul-ture engineered for syntrophic metabolite exchange are grown on membranes and then used to test LDPI-MS anal-ysis and imaging. Both E. coli strains displayed many sim-ilar peaks in LDPI-MS up to m/z 650, although some observed differences in peak intensities were consistent with the appearance of byproducts preferentially expressed by one strain. The relatively low mass resolution and accuracy of this specific LDPI-MS instrument prevented definitive assignment of species to peaks, but strategies are discussed to overcome this shortcoming. The results are also discussed in terms of desorption and ionization issues related to the use of 10.5 eV single-photon ionization, with control experi-ments providing additional mechanistic information. Final-ly, 10.5 eV LDPI-MS was able to collect ion images from intact, electrically insulating biofilms at ~100 μm spatial resolution. Spatial resolution of ~20 μm was possible,

although a relatively long acquisition time resulted from the 10 Hz repetition rate of the single-photon ionization source.

Keywords

Laser ablation · Mass spectrometry · Biological samples · Bioanalytical methods · Interface/surface analysis

Introduction

Biofilms are structured microbial communities encapsulat-ed in a self-produced extracellular polymeric matrix and are often organized as multispecies consortia composed of metabolically differentiated members interacting via ex-changed metabolites [1–3]. The biofilm phenotype is com-mon to many microbes and can occur on nearly any moist biotic and abiotic surface. Biofilms are ubiquitous and impact humans in many natural, medical, and industrial settings. Microbial colonization and biofilm formation on medical devices, such as catheters or implants, often result in robust and persistent infections. Additionally, infectious biofilms have been reported in dental, dermatological, and urinary tract settings [4]. Biofouling and biofilm-induced corrosion represent costly, negative effects within many in-dustrial settings including ship hulls, pipelines, and heat exchangers [2].

Biofilms are inherently tolerant of antimicrobial treat-ments [1, 2]. Several mechanisms have been proposed to understand this tolerance including metabolic dor-mancy, mass transfer limitation, phenotypic heterogene-ity associated with chemical gradients, and coordinated gene regulation via exchange of quorum sensing and other molecules [5, 6].

Mass spectrometry (MS)-based analyses of biofilms typ-ically rely upon homogenization and extraction, but an improved understanding of antibiotic resistance can be

gained via analysis of intact biofilms. Various methods in laser desorption have been applied to MS imaging of intact biofilms, including laser desorption postionization (LDPI) [7], matrix-assisted laser desorption ionization (MALDI) [8, 9], and laser ablation electrospray ionization (LAESI) [10]. Even ultrashort pulse lasers show potential for MS imaging of biological samples [11]. MALDI-MS imaging has many advantages for protein and peptide imaging, but it suffers from low ion to neutral ratios, location-specific ion suppression, and the need to add matrix. LAESI is advantageous for metabolites and does not require matrix addition, but desorption yield variations with water content require careful manipulation of analysis protocols [10, 12, 13]. Atmospheric pressure-based methods such as LAESI can also suffer from postionization ion-molecule reactions that lead to the formation of new ions that complicate spectral interpretation [14]. Finally, it is becoming increasingly clear that no single MS imaging method can detect all species present in a biofilm or any other type of intact biological sample.

Laser desorption postionization mass spectrometry (LDPI-MS) imaging has several potential advantages including matrix-free analysis, detection of the neutral desorbed fraction, and relative insensitivity to ion suppression [7]. LDPI uses vacuum ultraviolet (VUV) radiation to induce a relatively "soft" single photon ionization of laser-desorbed neutrals [15]. These characteristics combine to make LDPI-MS a complementary method to MALDI-MS, LAESI-MS, or other established strategies for MS imaging.

Prior studies of antibiotic-treated bacterial biofilms using a 7.87 eV photon energy VUV source found that antibiotics could be selectively detected from a large background of other desorbed species [7, 16]. However, biologically relevant molecules often have ionization energies higher than 7.87 eV [15, 17], requiring a higher photon energy source for their analysis. Prior LDPI-MS work with 8–24 eV VUV synchrotron radiation showed that higher photon energies dramatically improve sensitivity [18, 19]. For example, 12.5 eV photons produced significant parent ion signal, but fragment and other low mass ion signal was also enhanced at this relatively high photon energy. The 10.5 eV photon energy appeared to provide an optimal balance between improved sensitivity and minimal fragmentation for biofilm-antibiotic samples [18]. These finding encouraged the current work in which a pulsed 10.5 eV VUV source was implemented, based upon an established design [15, 20–22].

The 10.5 eV LDPI-MS imaging is demonstrated here for analysis and imaging of small endogenous molecules within intact biofilms. This study uses a model biofilm consortia comprised of a synthetic coculture engineered for syntrophic metabolite exchange [23]. The two coculture strains are well characterized for function and constitutively express two different fluorescent reporter genes to facilitate visual strain differentiation and analysis of localization. This synthetic biofilm consortium is ideal for development of LDPI-MS imaging for the exploration of fundamental biofilm behavior.

Experimental details

Bacterial strains Escherichia coli K-12 (MG1655) strains were used for all presented experiments. The cocultured biofilm system mimics a naturally occurring binary consortia relationship template of primary producer supported by a secondary consumer [23]. A glucose-consuming deletion strain (*E. coli* MG1655 *ΔaceAΔldhAΔfrdA, pRSET-mcitrine;* termed here as "citrine"), acts as the system's primary producer secreting organic acids as byproducts. A glucose-negative metabolically engineered strain (*E. coli* MG1655 Δ*ptsG*Δ*ptsM*Δ*glk*Δ*gcd, pRSET-tdtomato;* termed here as "tomato") acts as the organic acid scavenger. These strains constitutively express plasmids bearing their respective fluorescent reporter proteins (Dr. Tsien, UC, San Diego).

Medium All biofilms used in the reported experiments were grown in M9 media (6 g/L Na_2HPO_4, 3 g/L KH_2PO_4, 1 g/L NH_4Cl, 0.5 g/L NaCl, 1 ml/L of 1 M $MgSO_4{\cdot}6H_2O$) and 10 ml/L of trace metal stock solution (0.55 g/L $CaCl_2$, 0.1 g/L $MnCl_2{\cdot}4H_2O$, 0.17 g/L $ZnCl_2$, 0.043 g/L $CoCl_2{\cdot}6H_2O$, 0.06 g/L $Na_2MoO_4{\cdot}2H_2O$, 0.06 g/L $Fe(NH_4)_2(SO_4)2{\cdot}6H_2O$, 0.2 g/L $FeCl_3{\cdot}6H_2O$) [23, 24]. Carbon sources for the two strains were 10 g/L glucose for the primary producer strain (citrine) and 2 g/L sodium acetate for the scavenger strain (tomato). All stock solutions were either autoclaved or filter-sterilized. M9 agar plates (typically 15 g agar/L) contained 100 μg/mL ampicillin.

Biofilm growth and sample preparation Biofilms were grown on polycarbonate membranes (GE PCTE filter membranes, 09-732-18, Fisher Scientific) placed on agar medium. These membranes permitted nutrient access to the microbes via diffusion while providing suitable support for biofilm growth and subsequent MS analysis. Overnight cultures for tomato and citrine strains were prepared by inoculating experimental liquid media from either a fresh plate culture or frozen stocks. Tomato was grown in M9 minimal media with 2 g/L sodium acetate and 100 μg/ml ampicillin, and citrine was grown in M9 minimal media with 10 g/L glucose and 100 μg/ml ampicillin. Five to twenty percent *v/v* Luria-Bertani liquid medium was added to the M9-based growth media to ensure high culture densities (OD_{600nm}~ 0.1). The cultures were grown overnight for ~12 h at 37 °C.

Membranes were aseptically transferred onto separate agar plates. Typically, three membranes per plate were used, and each membrane was inoculated with diluted culture in exponential phase. For monoculture growth, 50 μL of culture was used, while 50 μL of each strain (1:1) was used for coculture growth. Inoculated membranes were allowed a short drying period in a laminar hood prior to incubation. The biofilms were grown for ~96 to 120 h at 37 °C. During this growth period, the membranes were aseptically transferred to fresh plates every 24 h. The final growth period varied depending on the desired thickness of the resulting biofilm. A few control experiments used biofilms doped with known species: 4-Dimethylaminopyridine was added directly to the agar media while 3,5-dibromotyrosine was added on top of the biofilms due to its low solubility.

MS instrumentation The schematic diagram in Fig. 1 displays the ion source region of the LDPI-MS instrument including the relative positions of the sample plate, lasers, and ion optics. The home-built reflectron time-of-flight mass analyzer was described previously [7]. The instrumental configuration in the ion source region differed somewhat from that described previously [7], but there are relatively few changes to the rest of the instrument. A Nd:YLF laser (Spectra-Physics Explorer, Newport Corporation, Irvine, CA) at 349 nm was used for desorption of microscopic portions of the sample for subsequent analysis in a custom-built LDPI-MS instrument. The energy used for desorption was typically 25–35 μJ, while the beam spot diameter was ~20 μm. The VUV ionization beams are shown for both the 7.9 and 10.5 eV photon energy sources, but only the latter was used in this study.

Figure 2 shows a schematic of the 10.5 eV (118 nm) source generation along with the ion source region of the LDPI-MS setup. The 10.5 eV radiation was generated by tripling the third harmonic of a Nd:YAG laser (~20 mJ, 5 ns, Tempest 10 Hz 355 nm, New Wave Research, Fremont, CA) in a Xe gas cell at 6.5 Torr pressure, similar to methods described previously [15, 20–22, 25]. The 355 nm radiation from the Nd:YAG laser was focused through a 200-mm focal length quartz lens (L1) to a custom-made, stainless steel Xe gas cell with high vacuum pumping, gas delivery, precision gauging, and integrated input and output optics mounts. The input window was antireflective coated quartz (for 355 nm normal incidence) while the output window was a VUV-grade LiF lens (L2) with 400 mm VUV focal length (±2 % at 120 nm, custom-made, Almaz Optics Inc., Marlton, NJ). Two steering mirrors (M1 and M2, highly reflective at 355 nm, 45° incidence) were used to direct the converging UV beam into the cell, and a quartz output window on the LDPI vacuum system mounted opposite the Xe gas cell allowed dumping of the 355 nm beam outside of vacuum, eliminating wall-generated ions and electrons while assisting alignment. This cell was evacuated to $<10^{-4}$ Torr with a turbomolecular pump and initially baked out, then filled with Xe gas to a pressure of 6.5 Torr as measured by a capacitance manometer. Tripling of the 355 nm beam was most efficient at this pressure, as gauged by acetone photoionization signal when the sample chamber and ion source region were back-filled with a constant pressure of acetone.

The time delay used between desorption and ionization lasers was in the range of 18–23 μs. The resulting photoions were extracted through large-bore Einzel lens that allowed efficient collection and transport of the large energy and spatial distribution from the ionized volume. Samples were mounted on an ultrahigh vacuum compatible precision translation stage (LS-120, Micos USA, Irvine, CA). A digital camera (Nikon D300) with macro lens (Nikon ED AF Macro Nikkor 200 mm 1:4 D) with a tilting adapter, for increasing the depth of view, was used to monitor the sample inside the vacuum chamber.

Data acquisition and processing MS data were acquired by a 12-bit, 125-MS/s plug-in data acquisition card (CompuScope

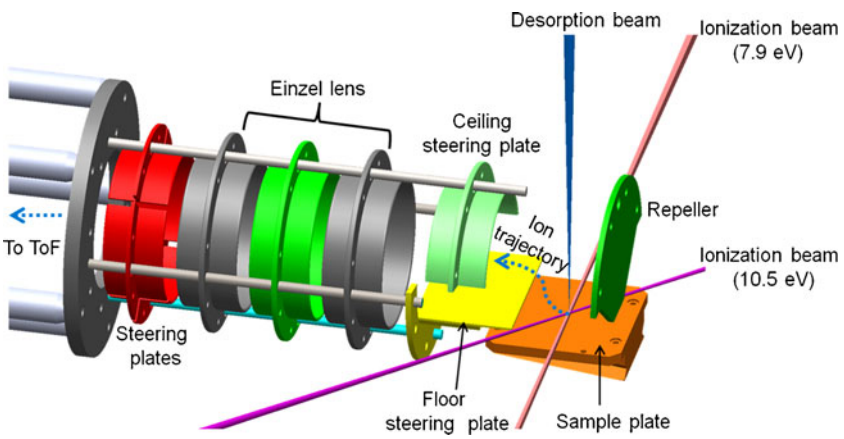

Fig. 1 Schematic of the ion optics of the LDPI-MS instrument as showing the sample plate, desorption, and ionization laser beams (*solid lines*), and the trajectory of the ions from the sample plate to the detector (*broken arrow*)

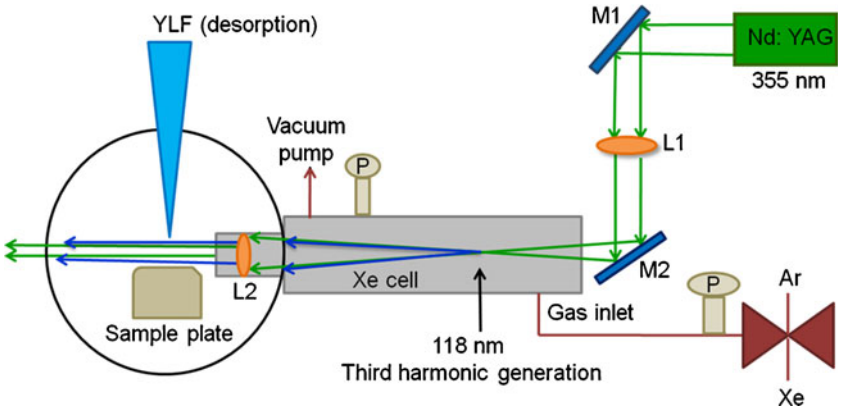

Fig. 2 Schematic of the 10.5 eV (118 nm) third harmonic generation source and ion source region of the LDPI-MS. *L1*, *L2*, *M1*, and *M2* denote lens 1, lens 2, mirror 1, and mirror 2, respectively

8229, Dynamic Signals LLC, Lockport, IL) using customized software for instrument control (LabView 2011, National Instruments, Austin, TX). The 10 Hz data acquisition rate was determined by the repetition rate of the Nd:YAG laser used to generate 10.5 eV VUV radiation. Data were collected continuously while the desorption laser scanned over the sample surface at a speed of 0.05 mm/s.

All of the data shown were the result of at least four replicates. Each mass spectrum shown was an average of $\geq 10^4$ laser shots, during which time the laser scanned an area of ~1 mm^2. Data were summed and plotted using commercial software (Origin 8.5) without any further processing. All spectra were mass-calibrated against standards.

Controls were performed to unambiguously correlate MS signal with species from the biofilm. For example, a desorption-only control was performed by blocking the photoionization laser beam while the desorption laser beam was used to collect background signal due to direct ionization. Controls performed by pumping out the Xe gas cell ruled out multiphoton ionization background due to the residual 355 nm YAG beam. The background signal from the membrane used to grow biofilms was also obtained: Polycarbonate membranes, used for growing biofilms, were incubated on agar plates without bacteria, for the same time as the biofilm samples under identical conditions, then measured as other samples. Peaks from biofilms were determined after carefully excluding the peaks from the above control measurements. For subtracting the two spectra, each spectrum was normalized to the peak noted. Difference spectra were normalized with respect to various peaks, but little change was observed in the result.

MS images were collected using an x–y translational stage (see above), where the stage meander establishing the sampling path was controlled by software. Meander speed and step width could be varied according to the image size and were determined by the required acquisition time. For the images presented here, the meander speed was ~0.3 mm/s with a step width of 100 μm, yielding an interpolated spatial resolution of ~100 μm. Images were processed and analyzed using free software (Biomap, www.maldi-msi.org).

Results and discussion

Mass spectra of cocultured E. coli biofilms Figure 3 (i) shows 10.5 eV LDPI-MS from the citrine (c), tomato (t), and mixed (m) regions of cocultured *E. coli* biofilms similar to that displayed in the inset photograph. Tomato and citrine strains were grown adjacent to each other on a single polycarbonate membrane sitting on an agar plate. The mass spectra shown in Fig. 3 were collected directly from each of the three noted regions of the same membrane after it was removed from the agar and placed in vacuum. Thus, biofilms were analyzed in their intact form on membranes without cell lysing, enzymatic treatment, or addition of any desorption-enhancing matrix.

Peaks at *m/z* 315.7±0.5, 525.8±0.1, 552.9±0.2, and 566.1±0.2 were tentatively assigned to fragments of phospholipids, based on previously reported laser desorption, fast atom bombardment [26], and electrospray ionization [27] studies of *E. coli.* Specifically, *m/z* 525.8 and 552.9 are thought to correspond to protonated fragments formed by loss of a phosphoethanolamine group from phosphatidylethanolamines with 18:0 and 16:0 fatty acid constituents, respectively. Parent ion peaks for these phosphatidylethanolamines were not observed and were assumed to be masked by background signal from the membrane. Gas chromatography coupled with electron impact ionization MS identified fatty acids present in *E. coli* membranes [28] and peaks corresponding to the molecular ion for several of the fatty acids were observed here. For example, the peak at *m/z* 284.8±0.3 and others in the *m/z* 50–220 range match the stearic acid parent ion and its fragment pattern (http://lipidlibrary.aocs.org). No assignments were

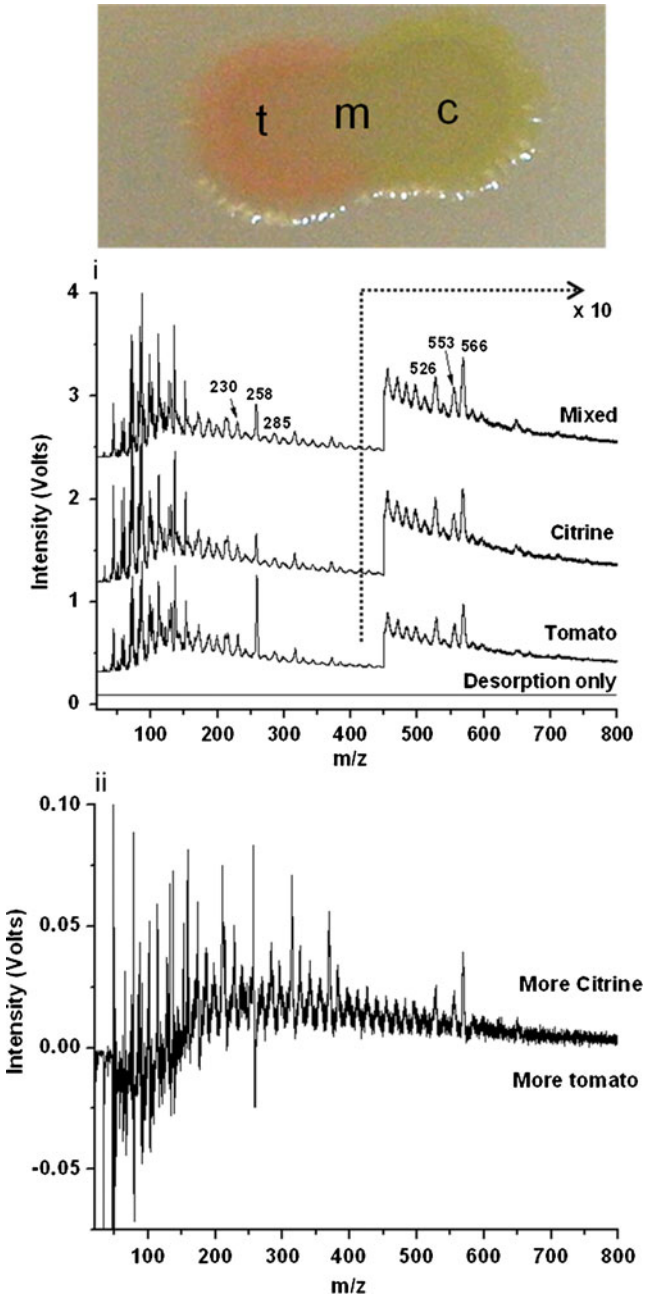

Fig. 3 *i* The 10.5 eV LDPI-MS of cocultured *E. coli* biofilm. The photograph at *top* shows the citrine strain region of the biofilm (*c*), tomato strain region (*t*), and mixed region where they overlap (*m*). *ii* The difference spectrum of tomato subtracted from citrine, following normalization at *m/z* 370. More citrine or more tomato indicates a region with higher signal in citrine compared with tomato and vice versa. Peaks marked with *m/z* values were more dominant in citrine, except for *m/z* 258, which was more dominant in tomato

made for the peaks at *m/z* 229.7±0.6, 258.2±0.5, 369.8±0.1, and 382.1±0.3.

The citrine, tomato, and mixed regions showed mostly similar peaks in their respective MS, albeit at differing intensities. Citrine showed overall higher MS signal intensity compared with tomato due to more robust growth on the glucose containing medium. A difference spectrum of the two monocultured regions grown under identical conditions on the same sample plate was generated to facilitate comparison: Fig. 3 (ii) shows the difference of the citrine MS after subtracting out the tomato MS (following normalization of both spectra to their respective peaks at *m/z* 370). The difference spectrum is mainly positive, indicating a higher overall signal for citrine compared with tomato. Several species above *m/z* 300 (especially those peaks marked with *m/z* values) were more dominant in citrine biofilms, although the *m/z* 258.2 peak was enhanced in tomato biofilms.

The generally higher signal for the citrine biofilm was consistent with the appearance of byproducts preferentially expressed by this strain. For example, enhancement of the peak at *m/z* 90 might arise from pyruvic and/or lactic acid, two previously observed citrine byproducts. Furthermore, other species and/or fragments thereof might also appear near *m/z* 90. While LDPI-MS can image microbial byproducts on intact biofilms (see below), correlation of ion signal with specific byproducts requires further verification.

Control measurements found no significant signal from either laser desorption only (see Fig. 3 (i) or postionization only, data not shown), indicating an absence of direct ionization (i.e., MALDI-like events) and single photon ionization of volatile species, respectively. While the LDPI-MS of the membrane alone did show a few peaks, those peaks appearing from biofilms at similar masses were excluded from further consideration. Laser-induced photoelectron ionization was also ruled out experimentally (see below).

Figure 4 shows the 10.5 eV LDPI-MS of a pure tomato strain biofilm at masses below *m/z* 160, showing a high density of peaks. For example, the peaks at *m/z* 88.1 and 90.1 were tentatively assigned to pyruvic and lactic acid, respectively, both known *E. coli* biofilm metabolites. However, the large number of possible endogenous species prevents definitive assignment of the low mass region of the spectra (see below). Figure 4 also shows the ~1,000 mass resolution possible with this LDPI-MS instrument from these relatively thick, high dielectric constant membranes. The mass resolution was improved in Fig. 4 (compared with Fig. 3) by optimizing the Einzel lens, steering, and reflectron voltages which also improved low mass signal at the expense of higher mass signal. By contrast, the spectra in Fig. 3 were recorded at lower resolution to obtain better signal to noise for the higher mass peaks.

The use of organic matrices for MALDI-MS analysis of bacterial biofilms often results in loss of information for the mass region *m/z*<300 due to strong matrix ion interference. Figure 4 demonstrates that LDPI-MS can be used to obtain information on low mass species inherent to the biofilm samples without the addition of any matrix. Preliminary results found that addition of a matrix compound to biofilms

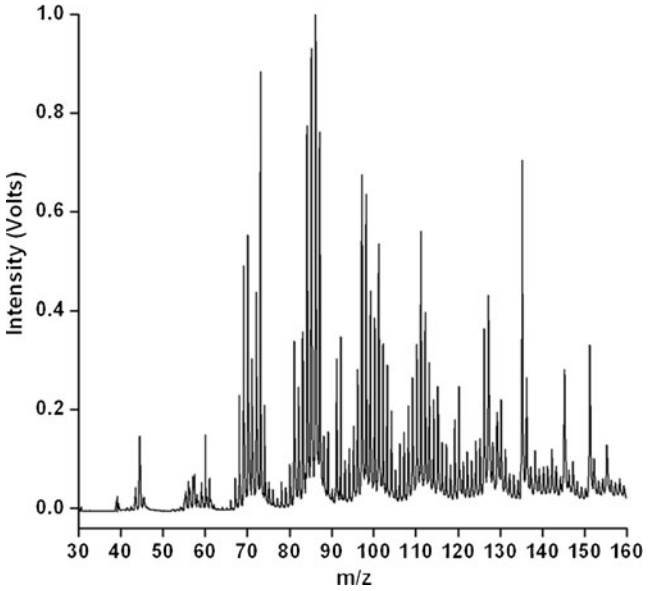

Fig. 4 The 10.5 eV LDPI-MS for tomato strain *E. coli* biofilm, optimized for low mass range *m/z* 30–160

only improved 7.87 eV LDPI-MS signal to noise by three to ten times, but the appearance of matrix ion peaks offset that advantage by obscuring adjacent masses from analysis [29].

Use of this and similar low-resolution, single analyzer instruments for LDPI-MS analysis of intact bacterial biofilms or other biological samples presents challenges in species identification similar to those encountered with secondary ion mass spectrometry [30]. The mass accuracy was calculated to be 340 ppm for Fig. 4, and there are over 10^3 known species whose singly charged parent ions would appear at *m/z* 150, with more species possible at higher masses [31]. The use of metabolomic databases for limited classes of species will dramatically reduce the number of candidate species at a given mass. Nevertheless, other strategies are still needed to assist compound identification with this particular type of LDPI-MS instrument. Post-acquisition data processing can be employed to improve effective mass accuracy, reducing the number of likely candidate species [30]. Culturing in media enriched in ^{15}N and/or ^{13}C stable isotopes will induce mass shifts facilitating compound identification [32]. Chemical derivatization followed by 7.87 eV single-photon ionization can selectively detect certain classes of species (see next section) [7]. Finally, solid-phase microextraction can be applied to purify the sample prior to collecting mass spectra [33], potentially employing blotting techniques to preserve spatial distributions.

Perhaps the most straightforward improvement in the LDPI-MS technique would be the addition of ion optics and an analyzer capable of tandem MS and/or high-resolution measurements. For example, there have been many instruments in which laser desorption was combined with postionization then coupled to a radio frequency ion trap [22, 34] or quadrupole-time-of-flight MS [10, 12, 13].

Imaging capabilities and performance of 10.5 eV source - Figure 5 shows the LDPI-MS image of an intact cocultured bacterial biofilm using 10.5 eV postionization. The software allows an image to be created from any range of masses: This image was constructed from a *m/z* 0.6 window around the *m/z* 258.2 peak, which showed higher signal from the tomato strain. Similar images could have been constructed which showed a brighter image for the citrine strain due to the higher abundance of other peaks (see Fig. 3). Again, the samples were analyzed directly on membranes without any sample preparation or addition of matrix.

The spatial resolution of the instrument was vibration-limited to ~20 μm. However, the spatial resolution of the image was degraded to collect the data in Fig. 5 by use of a large meander step size of ~100 μm, employed to allow the entire biofilm area to be imaged in ~90 min. This relatively long image acquisition time was due to the slow, 10-Hz repetition rate of the Nd:YAG laser used to pump the 10.5 eV source. However, this laser can be upgraded to a 30 Hz repetition rate, and similar lasers are available at repetition rates of 100 Hz or higher, dramatically speeding up data acquisition time.

The custom-built 10.5 eV source described here is compact, reliable, and easy to use. The 10.5 eV photons are generated reproducibly without further optimization if the 355 nm Nd:YAG laser is firing efficiently. The optical setup is simple and easy to align, allowing for direct measurement of the incoming 355 nm beam power. Prior estimates for conversion efficiency [25] indicate that the 10.5 eV output is in the low microjoule range. High vacuum pumping and an efficient gas delivery design make the baking out and purging of the cell both rapid and efficient. Furthermore, the source design simplifies the performance of control experiments used to rule out ablation by the desorption beam and multiphoton ionization from the residual 355 nm beam.

Desorption, fragmentation and ionization issues The instrument also has a 7.87 eV fluorine laser for more selective

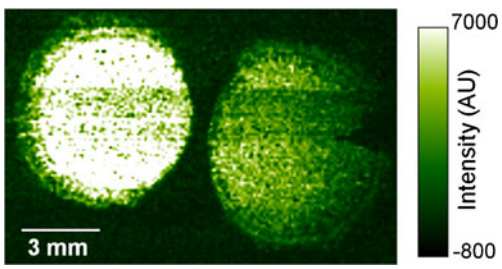

Fig. 5 The 10.5 eV LDPI-MS image of cocultured tomato (on *left*) and citrine (on *right*) strains of *E. coli* K-12 biofilms grown on polycarbonate membrane in glucose-containing minimal media. Image was plotted using ion signal at *m/z* 258.2±0.3. The intensity units are integers on a linear scale, where −800 corresponds to 0.0 V detector voltage and 7,000 corresponds to 1.07 V

single-photon ionization than is possible with 10.5 eV LDPI-MS. Single-photon ionization will occur for isolated molecular species with ionization energies below the photon energy [15]. Certain small molecules have sufficiently low ionization energies to allow 7.87 eV single-photon ionization, including many fused ring aromatics, tryptophan, and tertiary amines. However, most laser-desorbed species display ionization energies >7.87 eV and require 10.5 eV VUV to undergo single-photon ionization [15, 35]. Most amino acids, carboxylic acids such as saturated fatty acids with aliphatic carbon chains and phospholipids are excellent candidates for 10.5 eV single-photon ionization since they display ionization energies >7.87 eV [36]. However, 10.5 eV photon energy can somewhat increase ion fragmentation due to the excess photon energy above the ionization energy, leading to reduced parent ion intensity [15].

One potential source of ion fragmentation is 355 nm photodissociation of ions formed by 10.5 eV single-photon ionization, which is in principle possible since the 355 and 118 nm beams are coincident in this experimental configuration. Prior studies on a similar source ruled out photodissociation of ions when, as here, the 355 nm beam is defocused within the ionization region [25].

A more significant contribution to parent ion fragmentation is the transfer of desorption laser energy into internal energy of desorbed neutrals [22]. This energy transfer varies with multiple factors including laser pulse characteristics as well as optical and thermal properties of the target sample. Nevertheless, even slight changes in internal energy of gas phase species can enhance dissociation upon VUV single-photon ionization [37]. Paradoxically, higher laser power has been reported to reduce the internal energy of desorbed molecules via collisional cooling in the plume [38]. While dissociation via energy transfer during laser desorption can be considerable, it is also an issue in MALDI-MS [39].

Prior work that doped small molecular antibiotics in biofilms indicated desorption of molecular species up to at least ~1,500 Da occurs in LDPI-MS without the addition of matrix [7, 15, 16, 18]. Furthermore, LDPI-MS could detect a small amino acid doped in a polyelectrolyte multilayer designed to mimic the polysaccharides that are abundant in biofilms [17]. Again, no matrix was required for detection, although excessive desorption laser fluence did pyrolyze the polysaccharides.

A more complex issue is that of the mechanism of ion formation in LDPI-MS and how it might vary with VUV photon energy. The ionization mechanism in LDPI-MS has generally been considered to be single-photon ionization of isolated, neutral molecules that have been laser-desorbed into the gas phase, leading to the formation of radical cations [7]. The general rule has been that the photon energy must exceed the ionization of the analyte species to allow single-photon ionization.

However, other ionization mechanisms beyond single-photon ionization must also be considered. The lowered ionization energies of clustered molecules can allow single-photon ionization even when the ionization energy of the isolated molecule is up to ~0.3 eV above the photon energy [17]. Furthermore, dissociation of these clusters following single-photon ionization can form protonated species.

Another possibility is that protonation might occur via gas phase collisions in the desorbed plume following postionization. Such events might mimic the proton transfer from photoionized species to high-proton-affinity species that occurs in desorption atmospheric pressure (VUV) photoionization [40, 41]. Figure 6 shows the results of a test for proton transfer within a biofilm doped with both high and low proton affinity species, 4-dimethylaminopyridine (DMAP), and 3,5-dibromotyrosine (Br_2Y), respectively: Neither compound was appreciably protonated, with DMAP displaying the radical cation M^+ at *m/z* 122.2 and the signal at *m/z* 123.2 entirely attributable to the natural abundance of the ^{13}C isotope. The series of peaks near *m/z* 264.6 were previously identified as the most abundant ion in LDPI-MS of Br_2Y, a non-protonated fragment due to loss of NHCHCOOH, with the multiple peaks arising from the ~1:1 ratio of $^{79}Br/^{80}Br$ isotopes [17]. LDPI-MS of neat DMAP from a polycarbonate membrane (denoted "Analyte Neat") and 10.5 eV single-photon ionization MS of the relatively volatile DMAP subliming from the same membrane (denoted "No Desorption") also showed only M^+ and no protonated species. The ion-molecule reactions needed for protonation and that are known to occur in atmospheric

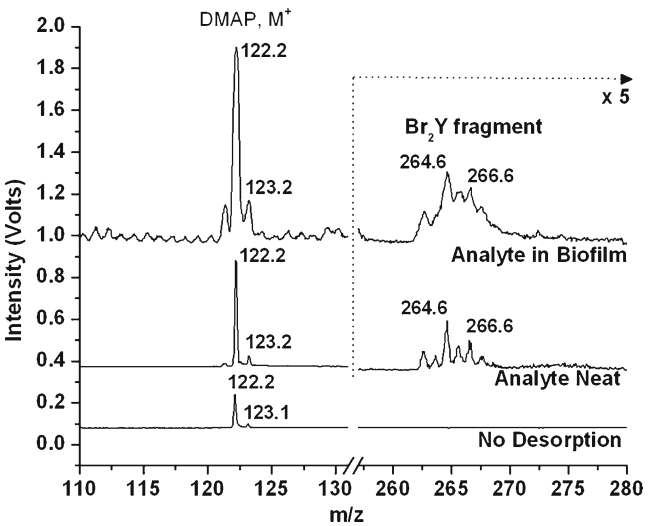

Fig. 6 *Top trace*: 10.5 eV LDPI-MS of citrine *E. coli* biofilms doped with 4-dimethylaminopyridine (DMAP) and 3,5-dibromotyrosine (Br_2Y). *Middle trace*: LDPI-MS of neat DMAP and Br_2Y on a polycarbonate membrane. *Bottom trace:* 10.5 eV single-photon ionization MS, without any laser desorption, of DMAP subliming from a membrane

pressure photoionization [14] are considered unlikely in LDPI-MS since the desorbed plume of neutrals is expected to expand too quickly into vacuum for the necessary postionization collisions.

Overall, it appears that formation of radical cations dominates LDPI-MS from biofilms. Several other potential ionization mechanisms are considered far less likely here. For example, laser-induced photoelectron emission from metal electrodes can lead to ionization [34] but was ruled out here by control experiments. Control experiments on gas phase ionization of acetone and LDPI-MS performed without Xe gas in the VUV generation cell ruled out UV-induced photoelectron effects. The absence of photoelectron effects is attributed to the collimated 10.5 eV beam from third harmonic generation of the coherent 355 nm Nd:YAG laser beam which is readily focused to avoid hitting any metal electrodes.

Conclusions

The 10.5 eV LDPI-MS possesses several advantages for small molecule imaging compared with other MS methods such as MALDI-MS [8, 9] and LAESI-MS [10]. For example, the ability to collect spectra without addition of desorption-enhancing matrix avoids signal fluctuation due to ion suppression, matrix inhomogeneity, and other quantification-inhibiting effects. Furthermore, 10.5 eV single-photon ionization cross-sections are within an order of magnitude of one another for a variety of species, facilitating quantification [15]. Quantification is likely better at 10.5 eV than at 7.87 eV, and other lower photon energies [42] since 10.5 eV is well above the ionization energy of most species [7]. The ability of LDPI-MS to collect images off of electrically insulating films shows promise for a wider variety of sample types than many other MS imaging strategies. Finally, the single-photon ionization mechanism of LDPI-MS is complementary to the protonation that dominates MALDI and LAESI. This complementary ionization indicates the three methods are likely to sample different molecular fractions from intact biological samples.

A variety of potential applications are foreseen with this instrument beyond metabolite analysis within intact biofilms. The detection of antibiotics and possible cell wall degradation products within intact biofilms by ≤10.5 eV LDPI-MS [18] indicates the additional potential for pharmacological studies in animal tissue. The 10.5 eV LDPI-MS has been used to detect cholesterol and other small molecules within intact animal tissue, complementing peptide analysis by MALDI-MS [11]. Lignin monomers and other important biomass components should be detectable by LDPI-MS since they have been measured using ion-sputtered rather than laser desorption [38, 43]. Work is beginning to show the quantification capabilities of LDPI-MS [42]. Finally, a variety of non-biological applications are envisioned for LDPI-MS imaging, such as analysis of chemical bonding within nanocomposite thin films [44].

Acknowledgments This work was supported by the National Institute of Biomedical Imaging and Bioengineering via grant EB006532. The contents of this manuscript are solely the responsibility of the authors and do not necessarily represent the official views of the National Institute of Biomedical Imaging and Bioengineering or the National Institutes of Health.

References

1. Costerton JW, Stewart PS, Greenberg EP (1999) Bacterial biofilms: a common cause of persistent infections. Science 284:1318–1322
2. Ghannoum M, O'Toole GA (eds) (2004) Microbial biofilms. ASM Press, Washington, D.C
3. Lopez D, Vlamakis H, Kolter R (2010) Biofilms. Cold Spring Harb Perspect Biol 2:a000398
4. Hatt JK, Rather PN (2008) Role of bacterial biofilms in urinary tract infections. Curr Top Microbiol Immunol 322:163–192
5. Stewart PS, Franklin MJ (2008) Physiological heterogeneity in biofilms. Nat Rev Microbiol 6:199–210
6. Straight PD, Kolter R (2009) Interspecies chemical communication in bacterial development. Ann Rev Microbiol 63:99–118
7. Akhmetov A, Moore JF, Gasper GL, Koin PJ, Hanley L (2010) Laser desorption postionization for imaging MS of biological material. J Mass Spectrom 45:137–145
8. Watrous JD, Dorrestein PC (2011) Imaging mass spectrometry in microbiology. Nat Rev Microbiol 9:683–694
9. Blaze M. T. M, Aydin B, Carlson RP, Hanley L (2012) Identification and imaging of peptides and proteins on *Enterococcus faecalis* biofilms by matrix assisted laser desorption ionization mass spectrometry. Analyst (in press). doi:10.1039/C2AN35922G
10. Vertes A, Hitchins V, Phillips KS (2012) Analytical challenges of microbial biofilms on medical devices. Anal Chem 84:3858–3866
11. Milasinovic S, Liu Y, Bhardwaj C, Blaze MTM, Gordon RJ, Hanley L (2012) Feasibility of depth profiling of animal tissue by ultrashort pulse laser ablation. Anal Chem 84:3945–3951
12. Nemes P, Barton AA, Li Y, Vertes A (2008) Ambient molecular imaging and depth profiling of live tissue by infrared laser ablation electrospray ionization mass spectrometry. Anal Chem 80:4575–4582
13. Nemes P, Woods AS, Vertes A (2010) Simultaneous imaging of small metabolites and lipids in rat brain tissues at atmospheric pressure by laser ablation electrospray ionization mass spectrometry. Anal Chem 82:982–988
14. Panda SK, Brockmann K-J, Benter T, Schrader W (2011) Atmospheric pressure laser ionization (APLI) coupled with Fourier transform ion cyclotron resonance mass spectrometry applied to petroleum samples analysis: comparison with electrospray ionization and atmospheric pressure photoionization methods. Rap Comm Mass Spectrom 25:2317–2326
15. Hanley L, Zimmermann R (2009) Light and molecular ions: the emergence of vacuum UV single-photon ionization in MS. Anal Chem 81:4174–4182
16. Gasper GL, Carlson R, Akhmetov A, Moore JF, Hanley L (2008) Laser desorption 7.87 eV postionization mass spectrometry of antibiotics in *Staphylococcus epidermidis* bacterial biofilms. Proteomics 8:3816–3821

17. Blaze MTM, Takahashi LK, Zhou J, Ahmed M, Gasper GL, Pleticha FD, Hanley L (2011) Brominated tyrosine and polyelectrolyte multilayer analysis by laser desorption VUV postionization and secondary ion mass spectrometry. Anal Chem 83:4962–4969
18. Gasper GL, Takahashi LK, Zhou J, Ahmed M, Moore JF, Hanley L (2010) Laser desorption postionization mass spectrometry of antibiotic-treated bacterial biofilms using tunable vacuum ultraviolet radiation. Anal Chem 82:7472–7478
19. Gasper GL, Takahashi LK, Zhou J, Ahmed M, Moore JF, Hanley L (2011) Comparing vacuum and extreme ultraviolet radiation for postionization of laser desorbed neutrals from bacterial biofilms and organic fullerenes. Nucl Instrum Meth Phys Res A 649:222–224
20. Arps JH, Chen CH, McCann MP, Datskou I (1989) Ionization of organic molecules using coherent vacuum ultraviolet light. Appl Spectr 43:1211–1214
21. Van Bramer SE, Johnston MV (1990) 10.5 eV photoionization mass spectrometry of aliphatic compounds. J Am Soc Mass Spectrom 1:419–426
22. Hanley L, Kornienko O, Ada ET, Fuoco E, Trevor JL (1999) Surface mass spectrometry of molecular species. J Mass Spectrom 34:705–723
23. Bernstein HC, Paulson SD, Carlson RP (2012) Synthetic *Escherichia coli* consortia engineered for syntrophy demonstrate enhanced biomass productivity. J Biotechnol 157:159–166
24. Miller JH (1972) Experiments in molecular genetics. Cold Spring Harbor Laboratory, New York
25. Oktem B, Tolocka MP, Johnston MV (2004) On-line analysis of organic components in fine and ultrafine particles by photoionization aerosol mass spectrometry. Anal Chem 76:253–261
26. Heller DN, Fenselau C, Cotter RJ, Demirev P, Olthoff JK, Honovich J, Tanaka T, Kishimoto Y (1987) Mass spectral analysis of complex lipids desorbed directly from lyophilized membranes and cells. Biochem Biophys Res Commun 142:194–199
27. Goodacre R, Heald JK, Kell DB (1999) Characterization of intact microorganism using electrospray ionization mass spectrometry. FEMS Microbiol Lett 176:17–24
28. Oursel D, Loutelier-Bourhis C, Orange N, Chevalier S, Norris V, Lange CM (2007) Identification and relative quantification of fatty acids in *Escherichia coli* membranes by gas chromatography/mass spectrometry. Rap Comm Mass Spectrom 21:3229–3233
29. Gasper GL (2011) MS imaging of antibiotics with *Staphylococcus epidermidis* bacterial biofilms by laser desorption postionization. Ph.D. thesis, University of Illinois at Chicago, Chicago
30. Pachuta SJ, Vlasak PR (2012) Postacquisition mass resolution improvement in time-of-flight secondary ion mass spectrometry. Anal Chem 84:1744–1753
31. Green FM, Gilmore IS, Seah MP (2011) Mass spectrometry and informatics: distribution of molecules in the Pubchem database and general requirements for mass accuracy in surface analysis. Anal Chem 83:3239–3243
32. Baran R, Bowen BP, Bouskill NJ, Brodie EL, Yannone SM, Northen TR (2010) Metabolite identification in *Synechococcus* sp. PCC 7002 using untargeted stable isotope assisted metabolite profiling. Anal Chem 82:9034–9042
33. Perera S, Berthod A, Dodbiba E, Armstrong DW (2012) Coupling solid-phase microextraction and laser desorption ionization for rapid identification of biological material. Rap Comm Mass Spectrom 26:853–862
34. Gamez G, Zhu L, Schmitz TA, Zenobi R (2008) Photoelectron emission as an alternative electron impact ionization source for ion trap mass spectrometry. Anal Chem 80:6791–6795
35. King BV, Pellin MJ, Moore JF, Veryovkin IV, Tripa CE (2003) Estimation of useful yield in surface analysis using single photon ionisation. Appl Surf Sci 203(204):244–247
36. Lias SG, Bartmess JE, Liebman JF, Holmes JL, Levin RD, Mallard WG (1988) Gas-phase ion and neutral thermochemistry. J Phys Chem Ref Data 17(suppl No. 1):18–25
37. Wilson KR, Jimenez-Cruz M, Nicolas C, Belau L, Leone SR, Ahmed M (2006) Thermal vaporization of biological nanoparticles: fragment-free vacuum ultraviolet photoionization mass spectra of tryptophan, phenylalanine-glycine-glycine, and β-carotene. J Phys Chem A 110:2106–2113
38. Kostko O, Takahashi LK, Ahmed M (2011) Desorption dynamics, internal energies and imaging of organic molecules from surfaces with laser desorption and vacuum ultraviolet (VUV) photoionization. Chem Asian J 6:3066–3076
39. Kim SH, Lee A, Song JY, Han SY (2012) Laser-induced thermal desorption facilitates postsource decay of peptide ions. J Am Soc Mass Spectrom 23:935–941
40. Luosujarvi L, Arvola V, Haapala M, Pol J, Saarela V, Franssila S, Kotiaho T, Kostiainen R, Kauppila TJ (2008) Desorption and ionization mechanisms in desorption atmospheric pressure photoionization. Anal Chem 80:7460–7466
41. Marchi I, Rudaz S, Veuthey J (2009) Atmospheric pressure photoionization for coupling liquid-chromatography to mass spectrometry: a review. Talanta 78:1–18
42. Blaze M.T. M, Akhmetov A, Aydin B, Edirisinghe PD, Uygur G, Hanley L (2012) Quantification of antibiotic in biofilm-inhibiting multilayers by 7.87 eV laser desorption postionization MS imaging. Anal Chem, submitted
43. Takahashi LK, Zhou J, Kostko O, Golan A, Leone SR, Ahmed M (2011) Vacuum-ultraviolet photoionization and mass spectrometric characterization of lignin monomers coniferyl and sinapyl alcohols. J Phys Chem A 115:3279–3290
44. Pleticha FD, Lee D, Sinnott SB, Bolotin IL, Majeski MW, Hanley L (2012) Acetylene ion-enhanced bonding of PbS nanoparticles to quaterthiophene in thin films. J Phys Chem C. doi:10.1021/jp306668k